18. R.B. Palmer, “Energy scaling, crab crossing and the pair problem”, SLAC-PUB-4707 (1988), Stanford (CA) USA.
19. A. Lehrach et al., “Modifications of the HESR layout for polarized antiproton-proton physics” Proc. of the 17th International Spin Physics Symposium SPIN2006, Kyoto Japan, AIP Conf. Proc. 915, 147 (2007).
20. A. Lehrach et al., “Polarized beams in the high-energy storage ring of the future GSI project”, Proc. of the 16th International Spin Physics Symposium SPIN2004, Trieste, Italy.
21. I. Koop et al.,”Longitudinally polarized electrons in Novosibirsk c-tau factory”, *J. Phys.: Conf. Ser.* 295, 012160 (2011).
22. A. Lehrach et al., “Overcoming depolarizing resonances at COSY”, AIP Conf. Proc. 667, 30 (2003).
23. K.Z. Khiari et al., Phys. Rev. 39, 45 (1989); H. Huang et al., Phys. Rev. Lett. 73, 2982 (1994); M. Bai et al., Phys. Rev. Lett. 80, 4673 (1998).
24. T. Roser et al., “Acceleration of polarized beams using multiple strong partial Siberian snakes”, Proc. of EPAC2004, Lucerne Switzerland, http://accelconf.web.cern.ch/AccelConf/e04/PAPERS/TUPLT190.pdf.
25. H. Huang et al., Phys. Rev. Lett. 99, 154801 (2007).

## 4.4 MEIC – A Polarized Medium Energy Electron Ion Collider at Jefferson Lab

Yuhong Zhang for the MEIC Study Group
Thomas Jefferson National Accelerator Facility, Newport News, VA 23606 USA
Mail to: yzhang@jlab.org

### 4.4.1 Introduction

Jefferson Lab’s response to U.S. scientific user demand for a future gluon microscope is to propose a high luminosity polarized medium energy electron-ion collider (MEIC). It is a natural expansion of the precision measurement based nuclear science program at Jefferson Lab, and opens new QCD research frontiers [1] with more than an order of magnitude increase in the center of mass (CM) energy coverage over the recent successfully completed 6 GeV CEBAF fixed target program, and the future 12 GeV CEBAF program after completion of the energy upgrade in 2015.

After over a decade of science and machine feasibility studies, the envisioned science program and accelerator technology developments have been driving this future electron-ion collider toward a medium CM energy range [2]. Currently, Jefferson Lab takes a two-step staging approach for this facility based on different CM energy coverage, namely, a low medium energy range and an upper medium energy range respectively, allowing a maximum science reach over the entire life of the proposed collider under the foreseen fiscal and technical constraints. During the last two years, the Jefferson Lab design effort has been focused primarily on the first stage, MEIC, with CM energy up to 66 GeV [3,4]. As a result of this effort, a conceptual machine design has been completed [5].

MEIC is currently designed as a ring-ring collider with up to three interaction points (IPs), enabling collisions of polarized electrons (and positrons) with polarized light ions (p, d, $^3$He and possibly Li and Be) and non-polarized light to heavy ions (up to lead). It covers beam energy up to 11 GeV for electrons, 100 GeV for protons and 40 GeV/u for

heavy ions. It utilizes the CEBAF linac for injection of a full-energy electron beam into a new storage ring. To complete the facility, a new ion injector and storage ring complex will be added to the Jefferson Lab site. For meeting one project goal, the option of a future upgrade is preserved for reaching 140 GeV CM energy and $10^{35}$ $cm^{-2}s^{-1}$ luminosity. Figure 1 shows the MEIC and its future upgrade in the Jefferson Lab site map.

Since the beginning of this study, the machine design effort has been focused on achieving the highest collider performance [6] in terms of high luminosities simultaneous over multiple IPs, full or very large detector acceptance capability, and high beam polarizations for leptons and several light ions. MEIC has adopted several unique design features to ensure the high performance. They include high bunch repetition rates and ultra small bunch charge ion beams; multi-staged electron cooling of ion beams; a figure-8 shape for all ion booster synchrotrons and both collider rings; and crab crossing of colliding beams at IPs. With these design features and other advanced accelerator technologies MEIC should be able to reach high luminosity above $10^{34}$ $cm^{-2}s^{-1}$ and also maintain 70% or above polarization for both beams.

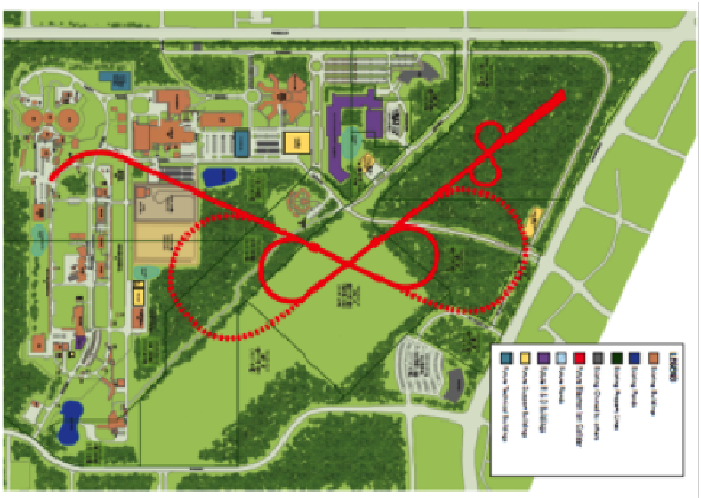

**Figure 1:** MEIC (solid red line) and its future upgrade (dashed red line) on the Jefferson Lab site. The ion injector (sources, linac and pre-booster) is in the upper right corner. CEBAF is on the left with a transfer line to the electron storage ring.

### 4.4.2 **Baseline Design**

The central part of the MEIC facility is two collider rings stacked vertically as shown in Figure 2. The electron ring stores 3 to 11 GeV electrons injected at full energy from CEBAF, while the superconducting ion ring stores 20 to 100 GeV protons or up to 40 GeV/u fully stripped ions. The two long straights of the figure-8 rings accommodate three IPs (the fourth symmetric location is reserved for a spin polarimetry); however, only two detectors are under consideration in the MEIC phase. As shown in Figure 2, the ion beams execute a vertical excursion to the plane of the electron ring for horizontal crab crossing at IPs. Such a design avoids the vertical motion of the electron beam for the purpose of preserving its low vertical emittance and spin polarization. An optional third detector may be placed at another IP for collisions of electrons with low energy (below 20 GeV/u) ions stored possibly in a dedicated compact storage ring.

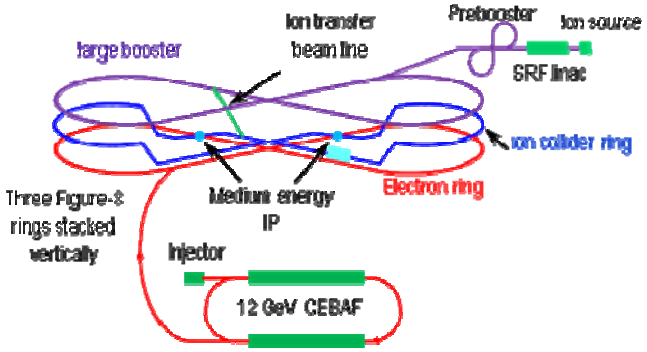


**Figure 2:** A schematic layout of MEIC at Jefferson Lab.

The MEIC machine parameters are summarized in Table 1 for *e-p* collisions at a 60×5 GeV$^2$ design point for both a full acceptance detector and a high luminosity detector (the values are in parentheses). Luminosities for *e-p* collisions with different CM energies are shown in Figure 3. Table 2 shows luminosity for *e-A* collisions for several representative ion species. To reach full detector acceptance, the magnet free detector space (the distance from an IP to the front face of the first focusing quad) must be at least 7 m for ions; however, it can be shortened to 3.5 m for electrons. For the second detector optimized for higher luminosities while still retaining a very large detector acceptance, the detector space can be reduced to 4.5 m so the luminosity is doubled to above $10^{34}$ cm$^{-2}$s$^{-1}$.

**Table 1:** MEIC Parameters at a design point of 60×5 GeV2 e-p collision for a Full-Acceptance Detector.

| | | Proton | Electron |
|---|---|---|---|
| Beam energy | GeV | 60 | 5 |
| Collision frequency | GHz | 0.75 | |
| Particles per bunch | $10^{10}$ | 0.416 | 2.5 |
| Beam current | A | 0.5 | 3 |
| Polarization | % | >70 | ~80 |
| RMS bunch length | mm | 10 | 7.5 |
| Normalized emit. ($\varepsilon_x$ / $\varepsilon_y$) | mm | 0.35/0.07 | 53.5/10.7 |
| Horizontal beta-star | cm | 10 (4) | |
| Vertical beta-star | cm | 2 (0.8) | |
| Vert. beam-beam tune-shift | | 0.015 | 0.03 |
| Laslett tune-shift | | 0.06 | Small |
| Detector space | m | ±7 (4.5) | ±3.5 |
| Luminosity per IP ($10^{33}$) | cm$^{-2}$s$^{-1}$ | 5.6 (14.2) | |

(Values for a high-luminosity detector are given in parentheses)

**Table 2:** MEIC *e-A* luminosities for different ion species.

| | | Proton | Deuteron | Helium | Carbon | Calcium | Lead |
|---|---|---|---|---|---|---|---|
| Ion species | | P | d | $^{3}He^{++}$ | $^{12}C^{6+}$ | $^{40}Ca^{20+}$ | $^{208}Pb^{82+}$ |
| Ion energy | GeV/u | 100 | 50 | 66.7 | 50 | 50 | 40 |
| Ion current | A | 0.5 | | | | | |
| Ions per bunch | $10^9$ | 4.2 | 4.2 | 2.1 | 0.7 | 0.2 | 0.05 |
| Ion β* (*x/y*) | | 6/2 (2.4/0.8) | | | | | |
| Ion beam-beam tune shift (vertical) | | 0.014 | 0.008 | 0.01 | 0.008 | 0.008 | 0.006 |
| Electron beam | Energy: 6 GeV; Current: 3 A; Electrons per bunch: $2.5 \times 10^{10}$<br>Vertical β*: 1.55 to 2.8 cm (0.61 to 1.1 cm)<br>Vertical beam-beam tune-shift: 0.022 to 0.029 | | | | | | |
| Luminosity/IP ($10^{33}$) | $cm^{-2}s^{-1}$ | 7.9 (20) | 5.5 (14) | 7.3 (19) | 5.5 (14) | 5.5 (14) | 4.4 (11) |

(Values for a high-luminosity detector are given in parentheses)

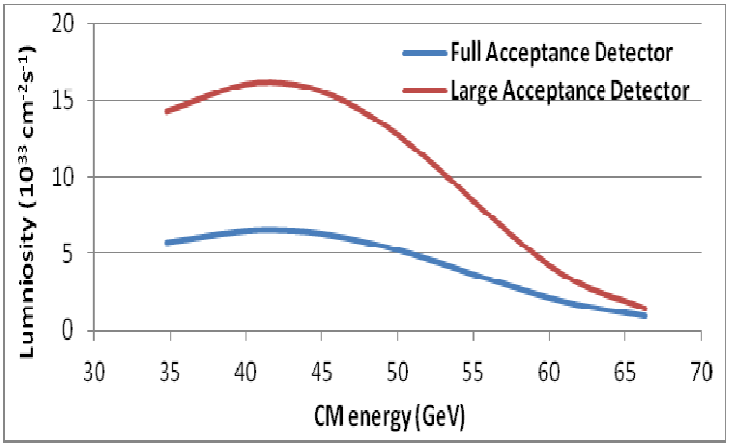


**Figure 3:** MEIC *e-p* collision luminosity.

### 4.4.3 Technical and Design Choices

The high luminosity of MEIC relies on high bunch repetition colliding beams [7], a key ingredient of a luminosity concept spearheaded by several modern lepton-lepton colliders [8] which have achieved unprecedented high luminosities. In MEIC, the electron beam from CEBAF has a bunch repetition rate of 1.5 GHz, while the ion beams from a specially designed ion complex will match the electron beams. MEIC thus holds a promise to replicate the luminosity success in colliders involving hadron beams. A 750 MHz has been chosen as a base frequency for the present design.

The MEIC collider rings stores several thousand ion or electron bunches with very small bunch spacing under a 750 MHz base frequency for the present design. The bunch charges of such beams are very small (as low as several of $10^9$ protons per bunch); however, a moderate current can be achieved by the large number of bunches in the rings. This is very different from a typical hadron storage ring whose bunch number is usually small; therefore the bunch length is usually long in order to hold a very large

number of particles (~$10^{11}$) per bunch for maintaining even a modest beam current. In MEIC, an ultra small bunch charge allows a dramatic reduction of the bunch length (as low as 1 cm RMS) with assistance of electron cooling, therefore permitting beta-stars hundreds times smaller than those of the typical hadron colliders. With appropriate interaction region designs, the combination of a high bunch repetition rate and ultra-small beta-stars could lead to a very high luminosity [7].

Initially, the Jefferson Lab electron-ion collider was designed naturally as an ERL-ring collider [9] due to the existing CEBAF SRF linac and also the successful experience of ERL technology. It later evolved into a traditional ring-ring collider after the realization that the ERL-ring collider scenario, in fact, does not provide additional and significant advantages in achieving a higher luminosity with high bunch repetition rate beams [7]. It would in actuality add tremendous burdens on technology development including high current polarized electron sources and high current/energy ERLs.

A unique design feature of MEIC is its figure-8 shape for all the booster and collider rings. Such a design greatly improves the preservation of the ion polarization during acceleration and storage, and also significantly simplifies the spin control [10]. An additional and important advantage of the figure-8 design is that it allows the acceleration and storage of polarized deuterons, thus expanding its science reach enormously [2].

The MEIC design is derived with certain limits on parameters of stored beams due to collective beam effects [5]: the ion beam space-charge tune-shift should be less than 0.1; the total beam-beam tune-shift summed over all the IPs must not be larger than 0.03 and 0.1 for ion and electron beams respectively. We have also imposed limits on other machine parameters [5] based largely on previous lepton and hadron collider experience and the present state of the art of accelerator technologies in order to reduce R&D challenges and to improve robustness of the design. As an example, the stored beam currents are up to 0.5 and 3 A for ions and electrons respectively, and the electron synchrotron radiation power should not exceed 20 kW/m.

### 4.4.4 **Electron and Ion Collider Rings**

The two collider rings have nearly identical footprints (shown in Figure 4) and intersect at two symmetric points in the two long straights of the figure-8 for medium energy collisions. The figure-8 has a crossing angle of 60°, thus partitioning the ring roughly equally into two arcs and two long straights. The long straights also accommodate utility components such as injection, RF systems, and electron cooling. There are two short (20 m) straights in the middle of the two arcs of the ion ring for two Siberian snakes. Table 3 summarizes the parameters of the ion and electron collider rings.

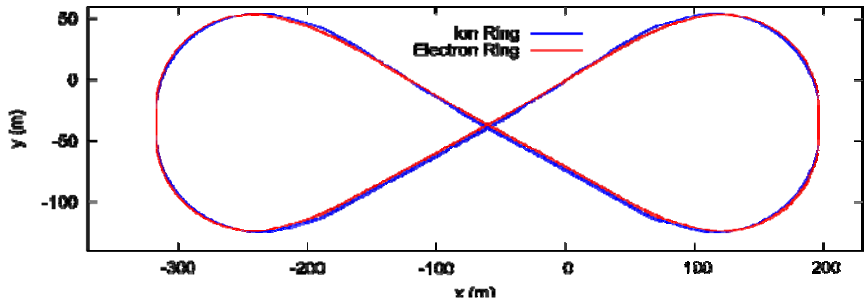


**Figure 4:** The layout of the MEIC electron and ion collider rings using MAD-X output.

**Table 3:** Main design parameters of the MEIC collider rings.

| | | Proton (ion) | Electron |
|---|---|---|---|
| Proton kinetic energy | GeV/u | 20 to 100 (40) | 3 to 11 |
| Circumference | m | 1340.9 | 1340.4 |
| Figure-8 crossing angle | deg | 60 | |
| Arc length[#] and average radius | m | 391.0 / 93.3 | 405.8 / 96.9 |
| Length of long and short straight | m | 279.5 / 20 | 264.5 / 25.9 |
| Electron universal spin rotator | m | | 47.6 |
| Base lattice | | FODO | |
| Length of cell in arc / straight | m | 9 / 9.3 | 5.25 / 5.58 |
| Phase advance per cell, hori. / vert. | deg | 60 / 60 | 120 / 120 |
| Number of cells in arc / straight | | 52 / 20 | 54 / 48.5 |
| Dispersion suppression | | Adjusting quadrupole strength | |

# An electron arc also includes short straight section and two Universal Spin Rotators

Both MEIC collider rings are designed as FODO lattices in arcs and straights. The functional blocks such as spin rotators, Siberian snakes, interaction regions and RF systems will be treated as isolated insertions into the base lattices and optics matching is required. The electron arc lattice is designed mirror symmetrically about the short straight in the center. Each half arc contains 27 cells including 2.5 and 3.5 cells for dispersion suppression near the short straight, and for matching optical functions to those of the spin rotator, respectively. The filling factor of the arc cell is 57%. There are 48.5 cells in one long straight; 5 of them are in two identical optics matching blocks at both ends. The electron ring optics function is shown in Fig. 5.

In the ion collider ring, the four 120º arc sections separated by two long and two short straights are designed identically with a FODO lattice. The 9 m long arc base unit is filled with two 3 m long SC dipoles of 3.236° bending; 33 such dipoles in one arc section provide 106.8° bending. Three more SC dipoles providing total 13.2° bending are placed 21 m away from the regular arc cells in order to match the footprint of an electron spin rotator. The ion collider optical functions are also plotted in Fig. 5.

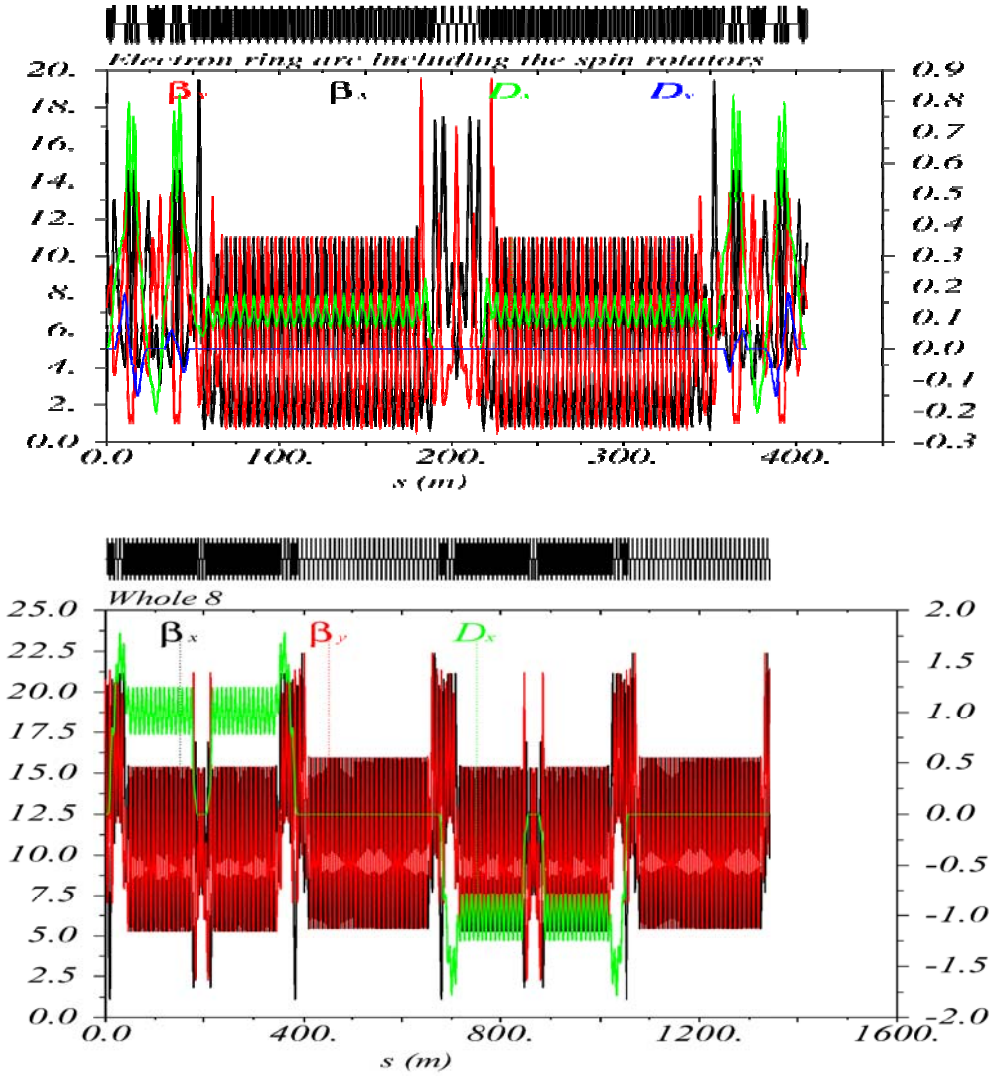


**Figure 5:** Optical functions of the electron (upper) and ion (lower) collider rings.

Beam synchronization in MEIC is a challenging issue. In the medium energy range, ions are not fully relativistic yet; thus the revolution time of the collider ring is energy dependent. On the other hand, electrons with energies of 3 GeV and above are already ultra-relativistic so the revolution time is a constant. The circumferences of two collider rings can be adjusted such that the revolution times are matched (or identical) for one particular ion energy. Nevertheless, this matched condition could not be maintained for the whole ion energy range. The beam synchronization problem can be further complicated with multiple IPs.

Presently, a scheme has been developed [5] for ensuring beam synchronization in the MEIC collider rings. It consists of two parts. At a sufficiently low (< 40 GeV) proton energy and over the whole range of heavy ions, variation of number of ion bunches (harmonic numbers) in the collider ring provides a set of discrete ion energies which satisfy the beam synchronization condition. For proton energy between 40 to 100 GeV, variation of electron ring circumference combined with variation of RF frequency provides a working solution. The main advantage of this scheme is that, being a normal

conducting magnet ring, the variation of the electron ring circumference is far easier since apertures of the magnets could be made large enough for a shift of the magnetic center up to 1.2 cm for one IP or 2.4 cm for two IPs. The scheme requires a variation of frequency of SRF modules by up to 0.012%. Though it has never been done before, it is believed achievable.

### 4.4.5 **Ion Injector**

The schematic layout [5] of the MEIC ion injector in Figure 6 illustrates the scheme [11] for ion beam formation and acceleration. The ions, coming out of the polarized or un-polarized sources, will be accelerated step-by-step to the colliding energy in the following machine components: a 285 MeV pulsed SRF linac, a 3 GeV pre-booster, a 20 GeV large booster and finally a medium-energy collider ring of 20 to 100 GeV. The energy values above are the design parameters for protons, and should be scaled appropriately for other ion species using a charge-to-mass ratio. All rings are in figure-8 shape for benefit of ion polarization.

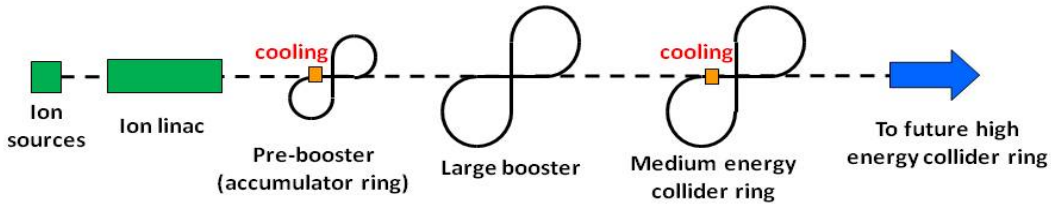


**Figure 6:** A schematic layout of MEIC ion injector complex.

The MEIC ion sources will rely on existing and mature technologies: an Atomic Beam Polarized Ion Source (ABPIS) with Resonant Charge Exchange Ionization for producing polarized light ions $H^-/D^-$ and $^3He^{++}$, and an Electron-Beam Ion Source (EBIS) currently in operation at BNL for producing unpolarized light to heavy ions. Alternatively, an Electron Cyclotron Resonance Source (ECR) can generate ions with 10 or more times charge per pulse than an EBIS source.

The technical design of a pulsed SRF ion linac, originally developed at ANL as a heavy-ion driver accelerator for FRIB [12] and shown in Figure 7, has been adopted for the MEIC proposal. Figure 8 shows the three types of SRF cavities used in this linac. This linac is very effective in accelerating a wide variety of ions from $H^-$ to $^{208}Pb^{30+}$.

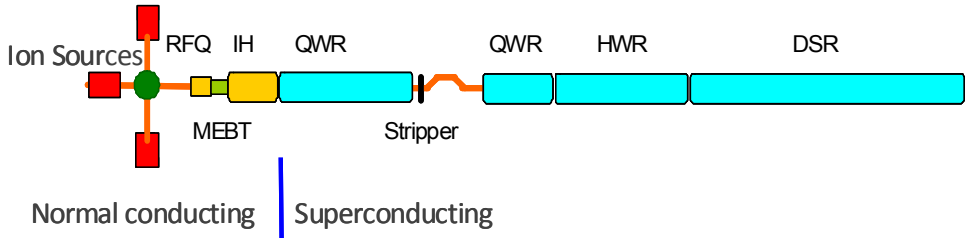


**Figure 7:** A schematic layout of the MEIC ion linac.

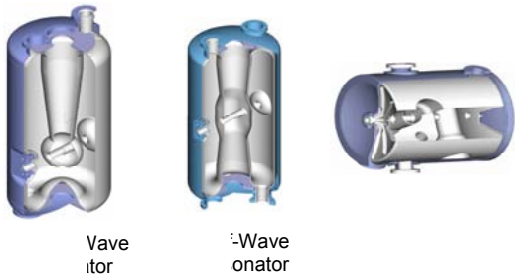


**Figure 8:** SRF cavities for the MEIC ion linac: quarter wave resonator (left), half wave resonator (center) and double-spoke resonator (right).

The pre-booster synchrotron accepts ion pulses from the linac, and after accumulation and acceleration, transfers them to the large booster. Figure 9 shows a layout of this pre-booster ring. It is designed [13,14] with three arc sections (two on the right side are identical) connected by two straights of the figure-8. The circumference of the pre-booster is one-fourth that of the large booster. The mechanisms of pre-booster operation depend on the ion species, relying on either the combined longitudinal and transverse painting technique for $H^-/D^-$, or conventional DC electron cooling for lead or other heavy ions during multi-turn injection from the linac. The optics design ensures a sufficiently high transition gamma such that the ions never cross the transition energy during acceleration in order to prevent particle loss associated with such crossing.

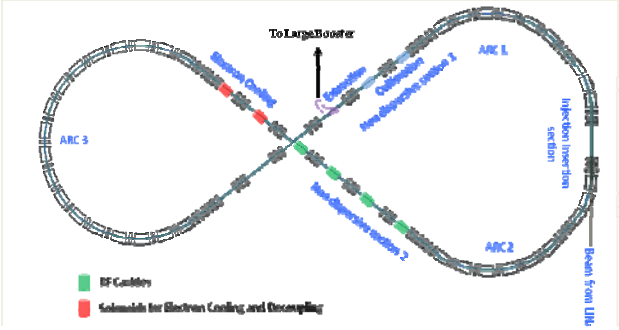


**Figure 9:** The layout of the MEIC pre-booster synchrotron.

The large booster synchrotron shares the tunnel with the collider rings, and will be responsible for accelerating protons from 3 to 20 GeV or ions with the same magnetic rigidity before transporting them to the collider ring. It is meticulously designed [15] to match the collider ring footprints including such special geometric features of electron spin rotators, ion Siberian snakes and interaction regions. The large booster has also adopted a FODO lattice as its base optics in the interests of simplicity and attaining relatively high transition energy. The latter is an important design goal for ensuring no crossing of the transition energy for any ion species, in order to avoid associated particle loss. The optics is broken down into large sections including four 120° arc sections, two long and two short straights, with optics matching between them and dispersion suppression at the end of each arc section. A preliminary analysis gives a dipole magnet ramping rate of 1.5 T/s; thus it takes 0.95 s to ramp the field to the peak value of 1.65 T. To boost the beam energy, two RF cavities, each having 120 kV voltage assuming it is operated at 45° off-crest, are placed in a dispersion free region of one long straight, requiring total 60 kW RF power [15].

### 4.4.6 **Electron Cooling and ERL Circulator Cooler**

MEIC has adopted a concept of multi-stage electron cooling of bunched medium energy ion beams [16,17]. First, low energy electron cooling will assist ion accumulation in the pre-booster. Next, in the collider ring, electron cooling is applied after injection, and then after the acceleration of ions to the collision energy for reduction of ion beam emittances and bunch length. Finally, cooling will be continued during collisions for the suppression of emittance growth induced by intra-beam scattering. Shortening the bunch length (1 cm or less) that results from electron cooling of the ion beam captured in a high voltage SRF field is critical for high luminosity in MEIC since it facilitates an extreme focusing and also crab crossing of the colliding beams at the IPs.

The multi-stage cooling scheme requires two electron coolers. One is a low energy cooler with a DC electron beam, based on mature technologies. The other is a medium energy cooler which demands new technologies for delivering a high current and high bunch repetition rate electron beam with energy up to 55 MeV. Presently this medium energy electron cooler is designed by utilizing several new technologies: a magnetized photo-cathode SRF gun, an SRF ERL, and a compact circulator ring [17]. A schematic drawing in Figure 10 illustrates this ERL circulator cooler design concept. These technologies play critical roles in the success of this cooling facility by providing most promising solutions to two bottlenecks of the facility: the high current and high power of the cooling electron beam. The first challenge is high RF power, up to 81 MW, for accelerating a 1.5 A, 55 MeV electron beam. Delivery of such high power without an ERL demands not only very high capital costs for hardware, but also unacceptably high operation costs. Furthermore, safely dumping a beam with such high power, about a hundred times that of the CEBAF 12 GeV beam, is technically unfeasible. With an ERL, nearly all beam power is recaptured in a decelerating pass and is then used for accelerating a new bunch. The second challenge is a need for a long cathode lifetime, in terms of the total extracted charge, which greatly exceeds the present state-of-the-art. A compact circulator ring, in which the cooling electron bunches will circulate multiple times while continuously cooling an ion beam, could lead to a reduction of beam current from the cathode by a factor equal to the number of circulations, thus extending the effective injector lifetime.

Currently, as a design optimization, this ERL circulator cooler is placed at the vertex of the figure-8 of the ion collider ring, as shown in Figure 10, by taking advantage of this unique shape. It provides two 30 m long cooling channels for gaining higher cooling rates.

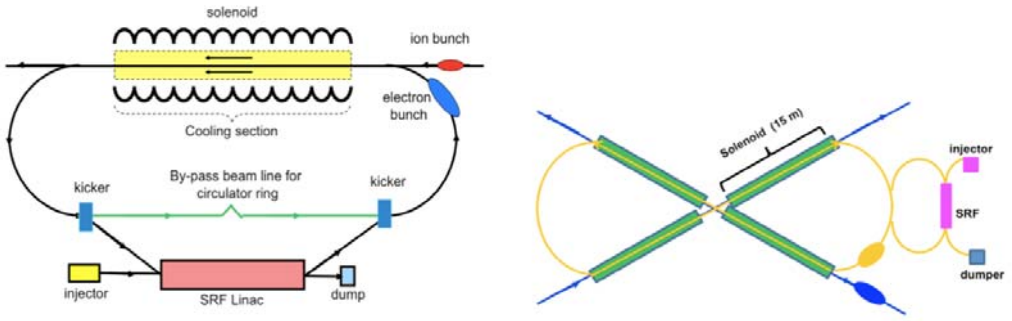


**Figure 10:** A schematic layout of an ERL circulator electron cooler (left) and an optimized location (right) in the MEIC ion collider ring.

Recently, a proof-of-principle experiment [18] has been proposed to demonstrate the ERL circulator cooler concept. The Jefferson Lab FEL is selected as the test facility for this experiment since it can provide a high quality electron beam with an energy range and bunch repetition rate similar to the cooler; therefore it allows maximum reuse of existing hardware, dramatically reducing the capital cost of this experiment. As shown in Figure 11, the presence of the two parallel IR and UV beam lines provides an opportunity for implementation of a compact circulator ring with two 180° bends already available. The purpose of this experiment is to demonstrate circulations of an electron beam in a circulator ring while the beam quality is satisfactorily preserved. Specifically, we will (1) demonstrate a scheme for bunch exchange between the ERL and the circulator ring, (2) develop and test support technologies such as ERL and faster kickers, (3) study beam dynamics and collective effects in the circulator ring, and (4) test bunch length change and longitudinal phase matching between the ERL and the circulator ring. We expect this experiment will be completed in less than three years.

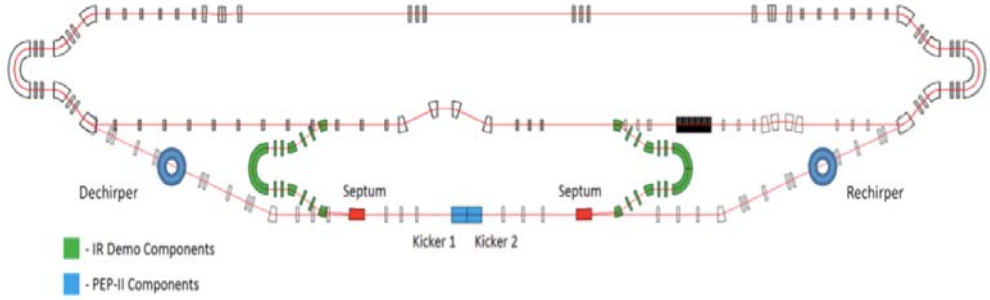


**Figure 11:** A test facility for an ERL circulator electron cooler.

### 4.4.7 **Polarization**

The unique figure-8 shape [5,10] for all the booster synchrotrons and collider rings is chosen for its advantage of preserving the ion polarization during acceleration and storage and for greatly simplifying the spin control. The mechanism is simple: the total spin procession (and the spin tune) in a figure-8 ring is zero. Further, a Siberian snake could shift the spin tune to a non-zero constant, thus retaining the energy independence, as a consequence, effectively by-passing all spin resonances during acceleration. Such a figure-8 design is also advantageous for the booster synchrotrons where polarization of protons and $^{3}He^{++}$ ions can be preserved by making the spin tune energy independent

with a partial snake if the space is too limited to accommodate full snakes, while this is not possible in a conventional circular synchrotron.

The figure-8 design is the only practical way [5] presently to preserve the deuteron polarization at the medium energy range. It allows acceleration and storage of polarized deuterons in a synchrotron, which is not possible in a circular synchrotron since the required Siberian snakes would be impractical due to the deuteron small anomalous magnetic moment.

The MEIC science program demands both longitudinal and transverse polarization of light ions at all IPs. Schemes for arranging ion polarizations in the two long straights (where one to two IPs are located) of the figure-8 collider ring have been developed [19]. For polarized protons and $^3He^{++}$ ions, three polarization configurations—namely, longitudinal at all IPs, transverse at all IPs, and alternately longitudinal in one straight and transverse in the other straight—are achievable, as illustrated in Figure 12. Using multiple Siberian snakes provides a high flexibility for science programs at the multiple detectors. For polarized deuterons, we can deliver a transverse polarization in both long straights; however, a longitudinal polarization is only possible in one straight while the spin orientation at the other straight will have an angle depending on the beam energy. Figure 13 illustrates the design of deuteron polarization in a figure-8 collider ring.

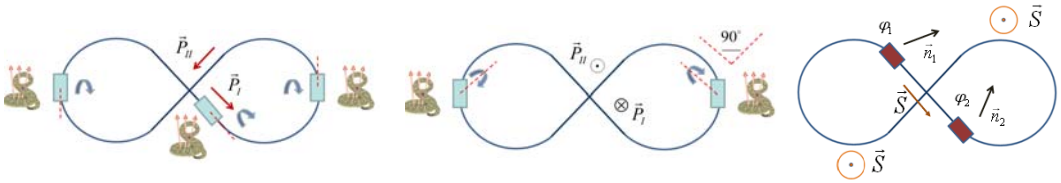


**Figure 12:** Polarization configurations of proton and $^3He^{++}$ ions in a figure-8 ring with Siberian snakes: longitudinal (left) and transverse (middle) polarization at all IPs. The right drawing shows a transverse polarization in one straight and a longitudinal polarization in the other.

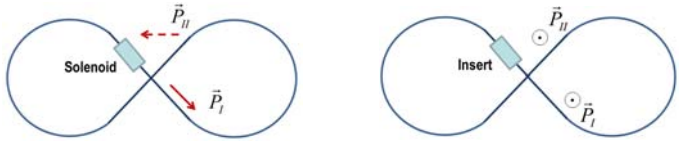


**Figure 13:** Polarization configurations of deuterons in a figure-8 ring with an SC solenoid or a special magnetic insert: longitudinal in one straight (left) and transverse polarization in both straights (right).

The MEIC electron ring also has a figure-8 shape since it is housed in a common tunnel as the ion collider ring. It should provide similar advantages to electron polarization after the future energy upgrade of MEIC, in which the electron energy will be ramped to 20 GeV in the ring. At the first stage, such advantages are not as significant or critical to the electron polarization as they are to the ion beam polarization.

In MEIC, the polarization of the electron beam originates in a polarized photo-cathode DC gun and can be easily preserved during acceleration in five passes of the CEBAF recirculating SRF Linac. CEBAF operations have shown that the polarization at 6 GeV is above 85%. It is expected that a similar high polarization will be achieved after the 12 GeV CEBAF upgrade. The design strategy of MEIC is to utilize the Sokolov-Ternov effect to preserve this high polarization and improve its lifetime in the

storage ring [5,20]. This requires aligning the electron spin in the vertical direction in arcs, and anti-parallel to the magnetic field of arc bending dipoles, as shown in the Figure 14. This, in turn, demands four energy-independent 90° universal spin rotators on each end of the two arcs to achieve longitudinal orientation at IPs. The first spin rotator rotates a downward spin to the longitudinal direction at one long straight; the second spin rotator then rotates the spin another 90° to upward orientation at the other half ring. This spin manipulation is repeated for the second long straight, and the electron will finally return to the original state of downward spin in the original half ring. The total spin tune is energy dependent, and to move the tune away from resonances, one or more spin tuning solenoids are placed in one long straight.

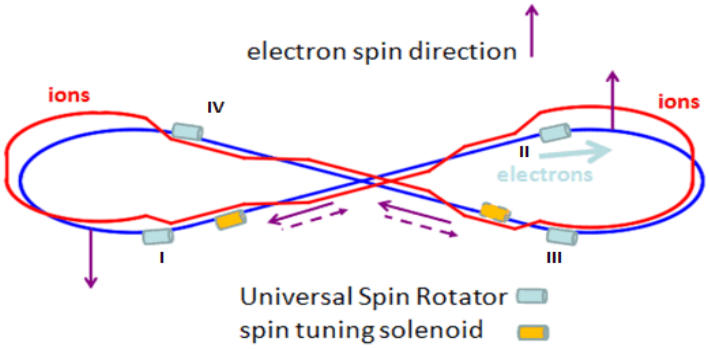


**Figure 14:** Illustration of spin orientation in the MEIC electron collider ring.

A concept of a universal spin rotator [5] has been developed to provide rotation of spin vectors. The term *universal* is used for referring its orbital and energy independence. As shown in Figure 15, it utilizes two solenoids and two (sets) of arc dipoles.

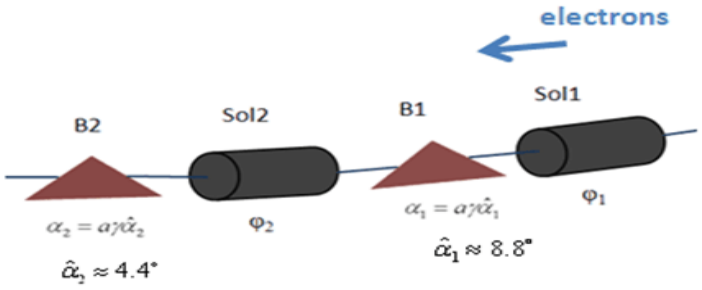


**Figure 15:** A schematic drawing of a universal spin rotator. B1 and B2 are the arc bends rotating spins by $\alpha_1$ and $\alpha_2$. Sol1 and Sol2 are solenoids with spin rotation angles $\varphi_1$ and $\varphi_2$.

### 4.4.8 **Interaction Region**

The design of the interaction region (IR) associated to the primary full acceptance detector is aimed for the detection of scattered electrons, mesons, and baryons without holes in the acceptance, even in forward regions, and operation in a high-luminosity environment with moderate event multiplicities and acceptable background conditions.

It should be pointed out that a full acceptance detector literally is capable of detecting particles with angles from 0 to 180°. The particles with a very small forward

angle (less than 1° with respect to the out-going ions), which are in abundance due to the high energy asymmetry of MEIC and carry rich information of great physical interest, are detected through a forward detector [21]. This new design concept allows these particles to pass through the apertures of the final focusing elements in an IR, and are then collected and analyzed by detectors placed after the final focusing block. Figure 16 shows the MEIC IR design that supports such forward particle detection.

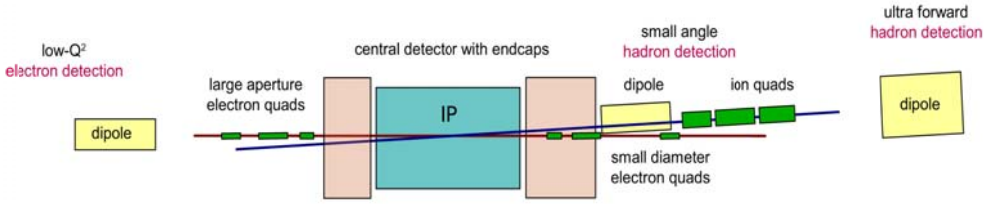


**Figure 16:** A layout of the interaction region of MEIC.

Additional issues were also taken into consideration in mapping the IR layout. Synchrotron radiation of the electron beam at or near the IR could cause serious background problems for the detector; thus bending of the electron beam in the IR has been minimized. It is designed such that the electron beam travels along a straight line (except inside a chromatic compensation block which has two weak dipoles for introducing and suppressing dispersion) after exiting the arc until reaching the IP. In the crab crossing scheme, the electron beam line is aligned with the detector solenoid, as shown in Figure 16. Further, to reduce the random background from the interactions between the ion beam and residual gas inside the beam pipe, the IPs are located as close as possible to the arc where the ion beam comes.

The MEIC IR consists of three function blocks, namely, final focusing block, chromaticity compensation block (CCB) and beam extension section, distributed from the IP toward the arc, with the optical functions for each block shown in Figure 17 for the ion beam. Figure 18 shows the optics functions over the complete ion and electron IRs [5].

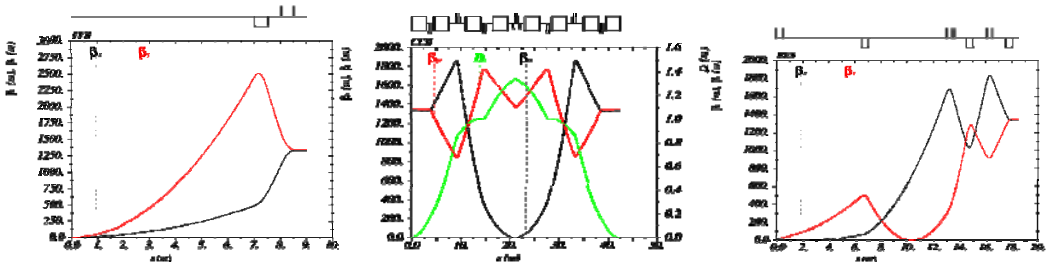

**Figure 17:** Optical functions of the ion beam at Final Focusing Block (left), Chromatic Correction Block (middle) and Beam Extension Block (right).

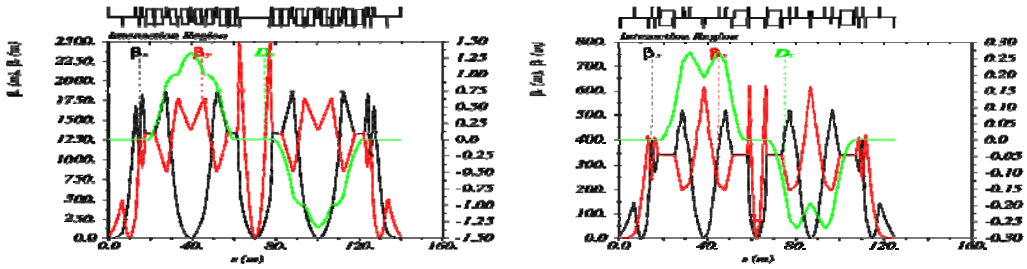

**Figure 18:** Complete optics of an ion interaction region (left) and electron interaction region (right).

A low-β insertion in an IR induces serious chromatic effects. The present approach of MEIC is a local correction scheme utilizing two CCBs placed on the both sides of an IP, as shown in Figure 18. A CCB for the ion beam is made of eight alternating horizontal dipoles sandwiched with seven quadrupoles, all arranged symmetrically as shown in the middle plot of Figure 18. The quadrupole strengths are adjusted to produce a total transfer matrix of the CCB that meets the symmetry requirements. Two sextupole pairs are inserted in each CCB; each pair is identical and placed symmetrically with respect to the center of the CCB. Such a scheme can simultaneously compensate the 1st order chromaticity and chromatic beam spot smear at the IP without inducing significant 2nd order aberrations [22].

For ion collider ring with two IPs, the horizontal and vertical chromaticities before compensation are - 278 and - 268, respectively. The strengths of two sextupole families in the CCB are adjusted to reduce slopes of the chromatic betatron tune curves to zero. As shown in the left plot of Figure 19, the tune variations are less than 0.005 and 0.01 in the horizontal and vertical directions respectively over a ± 0.2% range of $\Delta p/p$, and further within 0.02 and 0.03 over a wide $\Delta p/p$ range of ± 0.4% [9]. A frequency map analysis based on the tracking simulation results has demonstrated in the middle plot of Figure 19 that the momentum acceptance can easily reach ± 0.4%, about 14 times the ion beam momentum spread, with only the linear chromaticity compensation [23].

The dynamic apertures of the collider rings are explored by tracking particles for 1000 turns with increasing initial transverse amplitudes until a boundary between survival and loss is found. Simulations show the particles having large initial amplitudes experience stronger non-linear sextupole fields, resulting in a 3rd order aberration in the form of amplitude dependent tune-shifts [23]. Therefore, families of octupoles are introduced and placed in large betatron function but dispersion-free regions. These leave the linear chromatic correction unaffected, but compensate this 3rd order aberration. With this additional compensation, the dynamic aperture is increased significantly [23], as shown in the right plot of Figure 19.

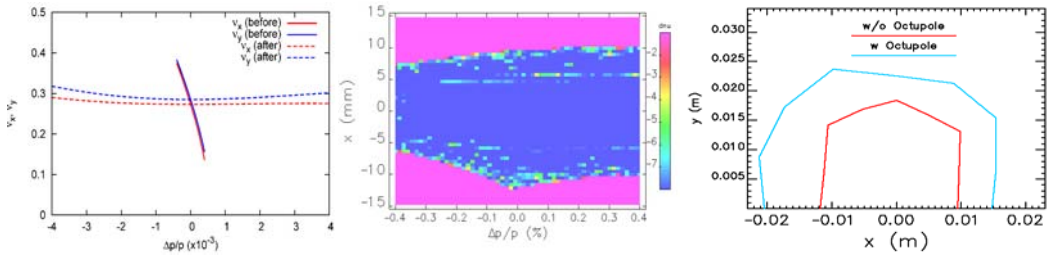


**Figure 19:** (Left) Chromatic dependence of the fractional betatron tunes before and after compensation. (Middle) Frequency map in the (x-Δp/p) space. The color reflects the tune change. (Right) Dynamic aperture of the ion ring without (red) and with (blue) octupole minimization of the 1st order amplitude-dependent tune-shift.

### 4.4.9 **Outlook**

MEIC is the primary future of the nuclear science program at Jefferson Lab beyond the 12 GeV CEBAF fixed target program. By incorporating several unique and advanced design features including figure-8 shape rings, staged electron cooling, and high bunch repetition rate beams, it holds a promise to deliver high performance including high luminosity above $10^{34}$ $cm^{-2}s^{-1}$ per detector for two IPs and higher than 70% polarization of electron and light ion beams. The two-step staging approach enables a physics program with CM energy range up to 66 GeV immediately and ultimately reaches a higher medium CM energy up to 140 GeV in a future upgrade. The first conceptual design of MEIC has been completed recently and a comprehensive design report is now available online and will be officially published soon.

The focus of the Jefferson Lab study group is now the accelerator R&D for both the technology development and demonstration and for beam physics studies. For the next two years, we will focus on the following topics: collective beam physics including beam-beam and electron clouds; election cooling simulation study and ERL circulator cooler technology development and demonstration; IR development and dynamic aperture optimization; and a demonstration of the advantages of the figure-8 ring on ion polarizations and a satisfactory electron polarization lifetime.

### 4.4.10 **References**


1. **"**Gluons and the quark sea at high energies: Distributions, polarization, tomography**",** D. Boer *et al*., arXiv:1108.1713 [nucl-th] (2011).
2. A. Accardi, V. Guzey, A. Prokudin and C. Weiss, "Nuclear Physics with a Medium-Energy Electron-Ion Collider", Eur. Phys. J. A 48: 92 (2012).
3. S. Ahmed, *et al.*, "Conceptual Design of A Polarized Medium Energy Electron-Ion Collider at JLab", Proceedings of PAC11, NY, NY, p2306 (2011).
4. S. Ahmed, *et al.*, "MEIC Design Progress", proceedings of IPAC12, New Orleans, LA (2012).
5. "MEIC - An Intermediate Design Report of A Polarized Ring-Ring Electron-Ion Collider at Jefferson Lab", edited by J. Bisognano & Y. Zhang (2012).
6. Ya. Derbenev, "Advanced Concepts for Electron-Ion Collider", Proceedings of EPAC 2002, Paris, France, p315, (2002).
7. Ya. Derbenev, G. Krafft, B. Yunn and Y. Zhang, "Achieving High Luminosity In An Electron-Ion Collider", Proceedings of HB2010, Morschach, Switzerland, p49 (2010).
8. For example, Y. Funakoshi, *et al.*, "Recent Progress of KEKB", Proceedings of

IPAC'10, Japan, p2372 (2010).
9. Ya. Derbenev, *et al.*, "ELIC at CEBAF", Proceedings of PARC2005, Knoxville, Tennessee, TPPP015 (2005).
10. Ya. Derbenev, "The Twisted Spin Synchrotron", University of Michigen Report UM HE 96-05 (1996).
11. S. manikonda, B. Erdelyi and P. Ostroumov, "Formation of Beams in the Accelerator Complex of The Medium Energy Electron Ion Collider Facility at JLab", Proceedings of IPAC12, New Orleans, LA (2012).
12. P. Ostroumov, *et al.*, "Design of the Driver Linac for the Rare Isotope Accelerator", Proceedings of HB2006, Tsukuba, Japan, p89 (2006).
13. B. Erdelyi, S. Mamnikonda, P. Ostroumov, S. Abeyratne, Y. Derbenev, G. Krafft and Y. Zhang, "An Accumulator/Pre-booster for the Medium Energy Electron Ion Collider at JLab", proceedings of PAC 2011, New York, NY, p1873 (2011).
14. S. Abeyratne, S. Manikonda, B. Erdelyi, "Design Studies of Pre-boosters of the Different Circumference for An Electron Ion Collider at JLab", Proceedings of PAC 2011, New York, NY, p954 (2011).
15. E. Nissen, T. Satogate and Y. Zhang, "The Design of A Large Booster Ring for the Medium Energy Electron-Ion Collider at JLab", Proceedings of PAC 2011, New York, NY, p954 (2011).
16. Ya. Derbenev, J. Musson and Y. Zhang, "Electron Cooling for a High Luminosity Electron-Ion Collider", Proceedings of COOL07, Kreuznach, Germany, p187 (2007).
17. Ya. Derbenev and Y. Zhang, "Electron Cooling for Electron-Ion Collider", Proceedings of COOL09, Lanzhou, China, p181 (2009).
18. Ya. Derbenev, D. Douglas, A. Hutton, G. Krafft , E. Nissen and Y. Zhang, "A Test Facility for MEIC ERL Circulator Ring Based Electron Cooler Design", Proceedings of IPAC12, New Orleans, LA (2012).
19. V. Morozov, Ya. Derbenev, Y. Zhang, P. Chevtsov, A. Kondratenko, M. Kondratenko and Yu. Filatov, "Ion Polarization in the Figure-8 Ion Collider Ring", Proceedings of IPAC12, New Orleans, LA (2012).
20. F. Lin, Ya. Derbenev, V. Morozov, Y. Zhang and D. Barber, "Electron Polarization in the Medium Energy Electron-Ion Collider at JLab", Proceedings of IPAC12, New Orleans, LA (2012).
21. V. Morozov, P. Nadel-Turonski, R. Ent and C. Hyde, "Integration of Detector into Interaction Region at MEIC", Proceedings of IPAC12, New Orleans, LA (2012).
22. V. Morozov and Ya. Derbenev, "Achromatic Low-Beta Interaction Region Design for An Electron-Ion Collider", Proceedings of IPAC12, New Orleans, LA (2012).
23. F. Lin, Ya. Derbenev, V. Morozov, Y. Zhang and K. Beard, "Optimization of Chromaticity Compensation and Dynamic Aperture in MEIC Collider Rings", Proceedings of IPAC12, New Orleans, LA (2012).